A Data-Driven Algorithm for Enabling Delay Tolerance in Resilient Microgrid Controls Using Dynamic Mode Decomposition

Gowtham Kandaperumal, *Member, IEEE,* Kevin Schneider, *Fellow, IEEE,* and Anurag Srivastava, *Fellow, IEEE*

***Abstract*—The increased implementation of smart grid technologies in the power distribution grid presents unique opportunities that enable resiliency, but also brings challenges motivating needs for novel solutions and mitigation techniques. The bi-directional power and data flow allow for the grid to operate with increased resiliency, which is the ability to avoid discontinuity of service to end-use loads during extreme events. However, in applications where control of the distribution grid or microgrid relies on communication networks, the degradation of communication systems in the form of loss or high latency can cause maloperation and result in loss of end-use loads. This paper presents a novel framework to enable delay tolerance of centralized microgrid control schemes to mitigate communication system latency impacts and guarantee successful control action. We demonstrate the delay tolerance on a control scheme that operates a battery energy storage system (BESS) to offset the sudden loss of generation and maintain system frequency. During periods of severely degraded communication system performance, the proposed delay-tolerant algorithm compensates for the latency by utilizing a data-driven model generated at the device level using dynamic mode decomposition (DMD) to determine the performance of the communications. The DMD technique predicts the system's frequency using device-level terminal measurements and provides updated control signals. The HELICS cosimulation platform evaluates the cyber-physical interaction of the power system model in GridLAB-D, the centralized control agent in Python, and the discrete network model in NS-3. The framework is tested and validated on the IEEE-123 node system modified to represent a networked remote microgrid model, and the results show an improvement in the dynamic performance of the control scheme when subject to communication delays.**

***Index Terms*—Microgrids, power distribution system, resilience, delay tolerant control, dynamic mode decomposition, data-driven.**

I. Introduction

RESILIENCY is increasingly becoming an essential attribute of the power grid in the wake of more frequent extreme weather events. There has been a focus on the decarbonization of the grid through the adoption of renewable technologies [1]. These renewable resources are non-dispatchable and contribute to more generation penetrating the power distribution system (PDS) at the grid's edge, thereby requiring advanced controls. However, the higher renewable distributed generation mix help greatly in the decarbonization of the grid. The infrastructure required to support increased renewable distributed renewable generation, decarbonization and resiliency capabilities has become more sophisticated and efficient to provide reliable power to the end-use loads. From a centralized transmission system with a producer-consumer model to a more decentralized and distributed prosumer model, the collective transformation of the PDS is driving an increased proliferation of advanced controls, energy management systems, sensor networks, computing resources, and communication infrastructure. All these upgrades are incremental steps towards the resilient and optimal control of the PDS.

Communication infrastructure can support various control techniques, including but not limited to, protection [8], Volt-VAR optimization [9], optimal dispatch of DERs [10], market-based controls [11], demand response [12], reconfiguration [13] and utility business operations [14]. The architecture of such communication-assisted control schemes in traditional PDS is largely centralized. Sensor networks send information to a centrally-located controller where the control process determines actuation requirements, and the actuation is wired back to the impacted device through a communication network. Alternative modes of control schemes viz. decentralized and distributed provide solutions to single points of failure in centralized control schemes.

Microgrids have shown great potential in enabling system resiliency [15] and are of great interest. The integration of communication systems to microgrids provides more significant avenues for optimal control but attaches another layer of susceptibility to the overall problem. In addition to providing resiliency to the system by increasing their ability to serve critical loads during high impact, low frequency (HILF) events, communication-assisted microgrid controls can be affected by the same phenomenon threatening the PDS (like hurricanes taking out communication back-hauls). Large-scale communication network failures have been reported following HILF events. Hurricane Maria left Puerto Rico with up to 95.6% and the U.S. Virgin Islands with 66.0% cellular communication sites out of service [16]. Another source of communication network delay stems from shared data traffic systems where these control algorithms operate through existing communication channels, thereby sharing bandwidth with other applications such as metering, SCADA, and enterprise data.

G. Kandaperumal was with the Washington State University, Pullman, WA and now working with the Regional Engineering at Commonwealth Edison, Aurora, IL, USA (email: gowtham.kandaperumal@comed.com).

A. Srivastava was with the Washington State University, Pullman, WA and now working with the Lane Department of Computer Science and Electrical Engineering at West Virginia University, Morgantown, WV, USA. (email: anurag.srivastava@mail.wvu.edu).

K. Schneider is with the Energy and Environment Directorate at Pacific Northwest National Laboratory, Seattle, WA, USA and with the Washington State University, Pullman, WA.

TABLE I
SUMMARY OF KEY RELATED WORK FOR COMMUNICATION-ASSISTED CONTROLS OF MICROGRIDS

Ref.	Controller architecture	Power system model	Communication system	Delay consideration
[2]	Hierarchical control	Canadian Urban Benchmark System - 9 nodes with 4 DGs	No communication system model	Modeled as constant transport delays of 0.1 s, 0.15 s, and 0.22 s
[3]	Distributed control	Laboratory setup with 2 DGs forming an islanded microgrid	No communication system model	Modeled as constant transport delays of 0.2 s, 1 s, and 2 s
[4]	Distributed control	Laboratory setup with 4 DGs forming an islanded microgrid	Communication system model modeled as graph	Link failure
[5]	Distributed Cooperative Control	Laboratory setup with 4 DGs forming an islanded microgrid	Sparse communication network	Link failure
[6]	Distributed control	Power system model modeled as graph	No communication system model	Not considered
[7]	Decentralized control	Laboratory setup with 4 DGs forming an islanded microgrid	No communication system model	Not considered
※	Hierarchical control and Local control	Unbalanced model of IEEE 123 node feeder	Star architecture with Point-to-Point links modeled in a discrete-event network simulator	Variable delay considered as result of network congestion in communication links

※This paper.

Earlier works have discussed the interdependence of communication system performance and the successful operation of power system controls. Reference [17] presents the formalization of the communication system adequacy to support power system applications. Reference [18] presents some baseline values for communication system latency in power system applications with delays between 40ms for digital fiber optics to above 100ms for analog radio channels. Some microgrid controllers affected by delays fail to realize their control objective successfully and lead to system failure. Reference [19] presents a cosimulation-based framework for the evaluation of power system dynamic performance under communication degradation. This work demonstrated the impact of communication system delays on delay-sensitive applications, in this case, the ability of a centralized controller to maintain the stability of a microgrid system through the dispatch of BESS resources during periods of photo-voltaic variability. The frequency regulation application of BESS in mitigating the variability of renewable generation is explored in [20] and design considerations in sizing and maintaining the life of utility BESS for rapid discharge applications are presented in [21], [22]. Typically, integrated PV-BESS systems use short-term forecasts to dispatch BESS in response to the uncertainties of PV generation [23]. However, in case of a sudden drop of PV generation, BESS can be utilized as a resiliency resource and dispatched to provide real power and frequency support. The reference [24] investigated such an use case and analyzed the impact of communication delay, packet loss, and packet manipulation on the resiliency performance of the microgrid. The work uses the HELICS cosimulation framework [25] to model the cyber-physical subsystems in different simulators and synchronize the simulations to study the interactions of the changes in each subsystem. The use case presented shows the loss of system resiliency due to increasing communication system delays. Since failure of such control application impact the overall operation of the critical microgrid (e.g. military base) and can directly lead to system failure, such applications can be considered mission-critical.

A power distribution/microgrid controller operating over a degraded communication system shows diminished performance [2]. In [3], [4], distributed microgrid controls are shown to exhibit some level of robustness to delays. Reference [5] shows distributed averaging as a viable concept to utilize sparse communication networks to achieve acceptable microgrid control performance in the face of communication failure. In [6], the authors provided a solution to high volume data traffic to obtain optimal power flow by proposing a distributed power management scheme that operates over low bandwidth wireless network with inputs from just two sensors, thereby reducing the data required for successful operation. The authors acknowledge that centralized schemes provide overall better performance at the cost of high reliability communication networks and do not comment about the impact of delays in the scheme. Another approach seen is to eliminate communication networks altogether, like in [7], where a decentralized control method for low-voltage DC microgrids is proposed without the need for communication links by considering unequal line resistances for enacting droop controls. These techniques, however, (a) do not apply to mission-critical applications, (b) assume fixed or no communication delays, and (c) require coordination between the different controlled devices. Other techniques like using high-reliability communications like point-to-point fiber optic links between controller and devices or adding redundancy are prohibitively expensive. A comparative analysis of communication-assisted controls in microgrid systems is shown in Table I.

We extend the work presented in [24] and incorporate the concept of delay-tolerance using a data-driven approach.

The key contributions of this work are:

1) Proposed a computationally fast, data-driven approach to facilitate a backup control action to achieve successful microgrid operation during periods of low communication performance.
2) Developed a Dynamic Mode Decomposition (DMD) based algorithm that utilizes terminal frequency measurements and dispatches a local setpoint for the BESS in the case of delayed actuation signals from the microgrid controller.

This article has been accepted for publication in a future issue of this journal, but has not been fully edited. Content may change prior to final publication. Citation information: DOI 10.1109/TSG.2022.3167436, IEEE Transactions on Smart Grid

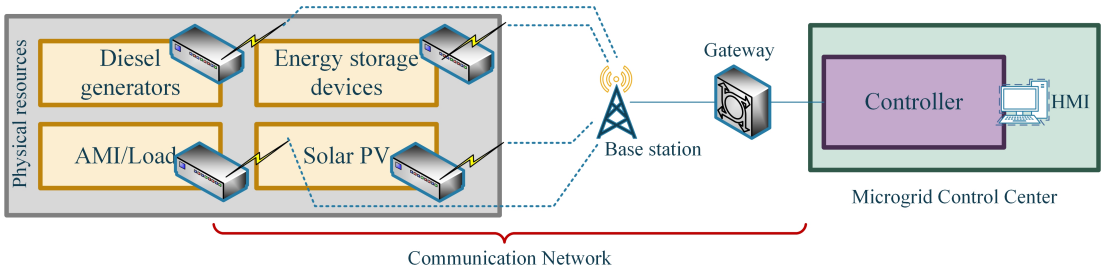

Fig. 1. Conceptual Model of Communication Assisted Controls in Microgrids

3) Established a proof-of-concept of achieving delay tolerance using measurement-based models to predict controller-communication network performance and correct deviation in control objectives by transferring control from centralized microgrid controller (MGC) to the local controller.
4) Developed a four model co-simulation setup to capture the interaction of the islanded microgrids, communication networks, communication assisted controls, and measurement based models.

Delay tolerance can be an important attribute for communication assisted controls for microgrids that are supported by legacy communication networks that do have high reliability. The data-driven methodology presented in this paper can help impart delay tolerance to such systems.

II. Delay Tolerance in Controls

Communication-assisted control actions are affected by the failure of the signal to reach on time (channel delay), loss of the signal in transit from the controller to the device (packet loss), or failure of the controller to present a valid control signal on time (process delay).

TABLE II
Methods to Enable Delay Tolerance in Smart Grid Applications

Delay tolerance approach	Specific measures
Communication techniques	Software defined networking
	Dynamic routing
	Distributed coordination
	Routing optimization
Optimization	Variable selection
	Approximation schemes
Control architecture	Distributed
	Decentralized
	Local autonomous
	Hybrid controls
Controller design	Robust
	Adaptive

Tolerance in this paper is defined as the "successful operation of the control action in spite of presence of significant communication system delays". Some causes of delays in smart grid communication networks include:

- Process delays due to increased data traffic volume
  - Communication link congestion from increased data traffic
  - Computation delays in communication nodes routing traffic
- Propagation delays due to physical constraints
  - Distance between nodes
  - Obstacles in line of sight communications
  - Electromagnetic interference from thunderstorms, solar flares, etc.
  - Physical loss of communication nodes
- Cyber-attacks
  - Network congestion attacks
  - Man in the middle attack

Some techniques to introduce delay tolerance in the system are shown in Table II. The advantage of using communication network techniques is lower cost due to the ad hoc nature of the solutions and increased efficacy of the delay reduction. Networking measures can also be leveraged for resilient controls by the restructuring of the communication networks during extreme events or cyber-attacks and providing cyber security [26]. This work, however, is agnostic to the source of the delay. We consider the proposed work a potential solution to maloperation caused by delays in critical microgrid applications, allowing the implementation of delay-sensitive applications over legacy and shared, high traffic communication networks.

III. Delay Tolerant Framework For Resilient Microgrids

Fig. 1 shows the conceptual model of communication-assisted controls in a typical networked microgrid system, where measurements and centralized control are enacted over a communication system. The microgrid grid controller dispatches the BESS when the loss of PV inverters increases real power mismatch. The following subsections will discuss the problem's setup and describe the individual subsystems involved in the proposed data-driven solution to delays.

A. Power System Model

A networked microgrid system is derived from a modified version of the IEEE 123-node test system. Three microgrids are delineated as shown in Fig. 2 with two microgrids having PV and BESS Inverter-based resources. The objective of the BESS is to offset the variability of PV and ensure that frequency limits are met during periods of low PV availability. The power system model is developed in the GridLAB-D

This article has been accepted for publication in a future issue of this journal, but has not been fully edited. Content may change prior to final publication. Citation information: DOI 10.1109/TSG.2022.3167436, IEEE Transactions on Smart Grid

simulation environment and provides detailed inverter, diesel generator (DG), feeder configuration, and end-use load models. GridLAB-D simulator solves the full unbalanced three-phase power flow using the method described in [27] and is run in delta-mode to observe the sub-second frequency response of the inverters and generators. Figure 3 shows the field implementation of the proposed setup.

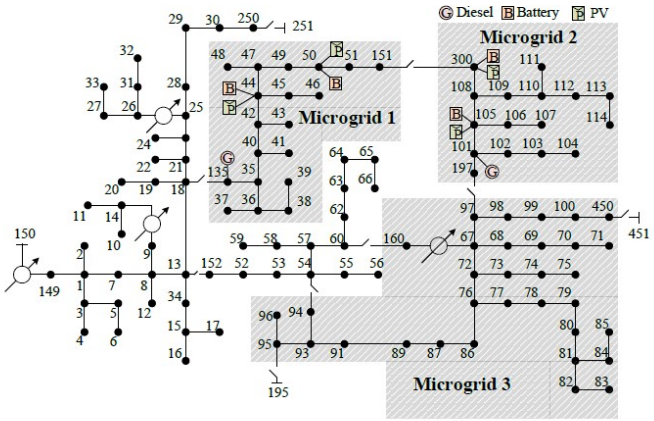

Fig. 2. Modified 123 node system representing networked microgrid architecture

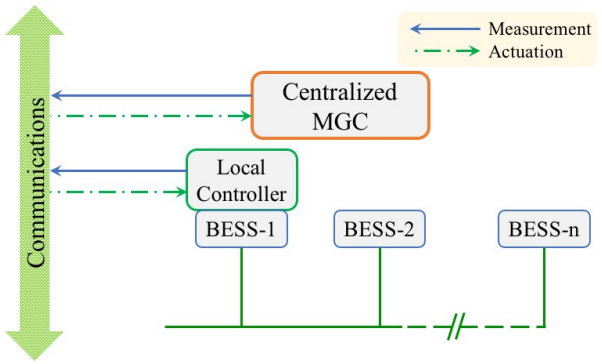

Fig. 3. Block diagram showing the field implementation of the proposed delay tolerant control scheme

Each BESS has a local controller that receives the individual BESS setpoints calculated by the centralized microgrid controller (MGC) and assesses the validity of the setpoint based on the data-driven model acquired by terminal frequency measurements. The power system model also has loads equipped with Grid Friendly™ Appliance (GFA) controllers with under-frequency load shedding (UFLS) function, which respond to frequency setpoints and shed in response to under-frequency events [28], thereby supporting the resilient operation of microgrids.

B. Communication System Model

Each DER in the microgrid setup is assumed to be attached to a communication node that can receive measurement signals from the DER or control signals from the centralized MGC. The communication networked is modeled in NS-3 as a simplified star architecture with the centralized MGC with point-to-point links connecting each measurement node to the MGC node. We assume that the communication channels also share data not specific to the application to be analyzed. To introduce delays in the communication network, we simulate a network congestion scenario where dummy nodes in NS-3 use shared point-to-point links to send and receive large volumes of junk data.

C. Centralized Controller

The control algorithm to mitigate the PV variability by dispatching BESS devices to offset said variability is presented in [24]. The authors in [24] present the algorithm as a method to respond to PV outage in electrically distant portions of the microgrid and to dispatch BESS fairly without stressing any specific device. The loss of PV causes a real power imbalance in the system and subsequently causes system frequency to drop. In such cases, the control algorithm calculates the power imbalance from measurement received remotely through communication channels, computes new dispatch set points for the BESS to offset the lost PV, and transmits the new setpoint as an actuation signal to the respective BESS inverters. The control algorithm is analogous to the secondary or tertiary frequency control in bulk power systems. The real power measurements from each DG, PV, BESS (represented as subscript B), and loads (L) is received by the controller, and the power imbalance ΔP_{Imb} is computed as,

$$\Delta P_{Imb} = \sum_{i=1}^{N_{DG}} P_{DG}^{i} + \sum_{j=1}^{N_{PV}} P_{PV}^{j} + \sum_{k=1}^{N_B} P_B^k - \sum_{l=1}^{N_L} P_L^l \quad (1)$$

For each BESS B^k with a rating of $P_B^{k,R}$, the available flexibility margin, $\overline{\Delta} P_B^k$, is calculated as,

$$\overline{\Delta} P_B^k = P_B^{k,R} - P_B^k \quad (2)$$

The centralized controller computes the new BESS setpoints to compensate for the drop in generation, by maintaining the combined output of the PV generation and BESS output near set value maintaining the frequency within the acceptable limits. The BESS dispatch coefficient α_k, which is computed from the available margin, provides a new setpoint to individual BESS resources without stressing any particular BESS.

$$max \cdot \sum_{k=1}^{N_B} \alpha_k * \Delta P_B^k \quad (3)$$

subject to the following constraints:

$$\begin{aligned} \sum_{k=1}^{N_B} P_B^k &= \Delta P_{Imb} \\ \Delta P_B^k + P_B^k &\leq \Delta P_B^{k,R} \\ \Delta P_B^k &\leq \frac{\Delta P_{Imb}}{\sum_{k=1}^{N_B} \overline{\Delta} P_B^k} * \overline{\Delta} P_B^k \end{aligned} \quad (4)$$

This article has been accepted for publication in a future issue of this journal, but has not been fully edited. Content may change prior to final publication. Citation information: DOI 10.1109/TSG.2022.3167436, IEEE Transactions on Smart Grid

The α_k term is a scalar that is proportional to the available dispatch margin of each individual battery and inversely proportional to the total power imbalance.

$$\alpha_k = \frac{\overline{\Delta} P_B^k}{\Delta P_{Imb}} \tag{5}$$

Once α_k is computed, the dispatch signal for each battery is relayed to the corresponding BESS via the communication link.

D. Terminal Controller

The proposed framework uses frequency prediction from the DMD algorithm based on the data-driven model derived from successful historical control. A voltage source inverter (VSI) control is utilized where the inverter emulates a synchronous machine and dispatches a new real power setpoint based on the droop. The droop equation for frequency regulation is,

$$f - f^0 = -k_p(P_B - P_B^0) \tag{6}$$

f^0 and P_B^0 are the nominal frequency and momentary battery setpoints. The frequency droop control characteristics are shown in Fig. 4.

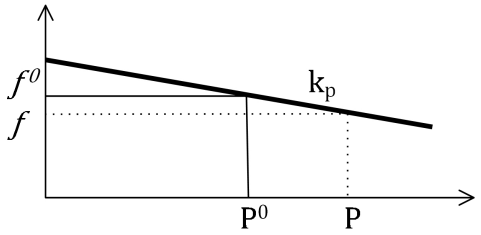

Fig. 4. Frequency droop control characteristics

E. HELICS co-simulation Platform

Each simulator used in this work is integrated into the HELICS co-simulation platform [25]. HELICS is an open-source, flexible, scalable framework that allows for the integration of multiple federates such as the setup used in this work. We use GridLAB-D for the distribution system power flow simulation, NS-3 for communication network simulation, and Python to simulate the control algorithms. The setup of the co-simulation is presented in Fig. 5.

HELICS provides time coordination for all the federates and facilitates message passing between the resources in GridLAB-D and the controller agents in the centralized controller. Each measurement and control point in GridLAB-D is initialized as a message federate. The message federate definition uses endpoints to send measurements and dispatch setpoints between the GridLAB-D, NS-3, and python simulators. Since the GridLAB-D and NS-3 simulators operate at different time steps, the HELICS broker allows the simulators to advance, only halting to synchronize as necessary or if messages are

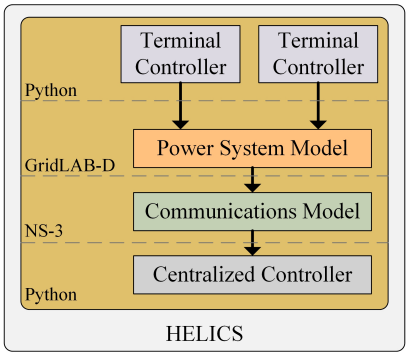

Fig. 5. Federate setup for co-simulation

sent or received. Figure 6 shows the overview of the proposed work. The simulation module (GridLAB-D) runs the power flow and dynamic simulation for the IEEE 123 node feeder based microgrid model. The data, observer and controller modules are coded in python. The data model performs the DMD based frequency prediction, explained in the following section. The observer module makes the decision if the inverter needs to work based on the dispatch signal from the centralized remote controller or the local controller using terminal measurements. The dispatch signals that are calculated by the remote controller are relayed via the NS-3 communication network.

F. Dynamic Mode Decomposition

The fundamental idea forming the basis of the proposed framework is the use of a data-driven model of the dynamic system to forecast system states that indicate the successful or unsuccessful operation of the control algorithm. We assume that the deviations from the forecasts presented by the data-driven model and the terminal measurements seen at the inverter device are primarily due to maloperation caused by communication system delays. The time-series frequency measurement at the terminal of the inverter device is collected for the successful operation of the control algorithm and serves as the baseline data for developing the data-driven model. The data-driven model is derived via *Dynamic Mode Decomposition* (DMD) [29]. The eigenvalue decomposition of DMD allows for spectral analysis of the linear dynamics of the system. The time-series data used to derive the model of a successfully controlled system is the terminal frequency measured at the BESS inverter. The DMD creates a forced linear system approximation of the dominant modes and frequency of the non-linear frequency measurements. These modes and frequencies are approximations of the modes and eigenvalues of the Koopman operator K. The DMD of the univariate time series analysis of frequency is performed as follows:

1) Hankelization: The time series terminal frequency measure $f = [f_1, f_2, \ldots, f_N]$ is univariate with N measurements and is assumed to be contaminated with measurement noise. The first step in recovering the dominant signal of interest is to use projective subspace techniques to remove noise contribution to the signal [30]. Time embedding of f transforms the univariate

This article has been accepted for publication in a future issue of this journal, but has not been fully edited. Content may change prior to final publication. Citation information: DOI 10.1109/TSG.2022.3167436, IEEE Transactions on Smart Grid

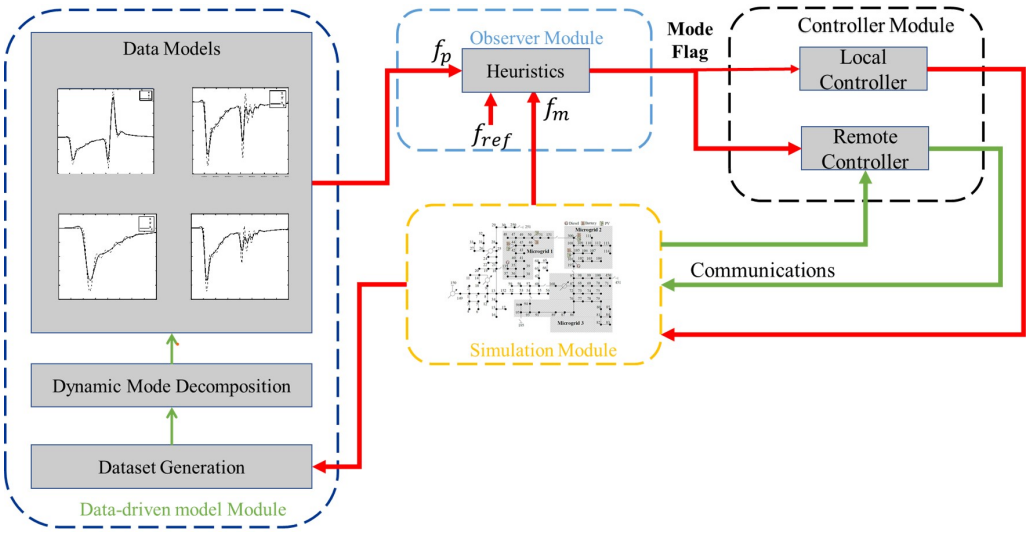

Fig. 6. Overview of Proposed Work to Enable Delay Tolerance in Smart Grid Applications

vector into a multi-dimensional trajectory matrix $\mathbb{F}$ of size $K \times L$.

$$\mathbb{F} = [\overline{f}_1, \overline{f}_2, \ldots, \overline{f}_L] \in \mathbb{R}^K \tag{7}$$

$$\overline{f}_n = [f_n, f_{n+1}, \ldots, f_{n+K-1}]^N \tag{8}$$

where $L \in [2 \leq L \leq \frac{N}{2}]$ and $K = N - L + 1$. The trajectory matrix $\mathbb{F}$ is a Hankel matrix and now can be used to derive a matrix $\mathbf{K}$ that maps the $\overline{f}_n$ vector to $\overline{f}_{n+1}$. The linear operator $\mathbf{K}$ advances the dynamics one time step forward.

2) Dynamic Mode Decomposition: The matrix $\mathbf{K}$ connects the k-lagged vector at timestep n to the next time step n+1 is the mapping matrix called the Koopman Operator. Since $\mathbf{K}$ is a $K \times K$ matrix, the solution of $\mathbf{K}$ is computationally expensive. The dimensional reduction of $\mathbf{K}$ can be achieved through the DMD at this point [31].

$$\mathbf{M} = [\overline{f}_1, \mathbf{K}\overline{f}_1, \mathbf{K}^2\overline{f}_1, \ldots, \mathbf{K}^{N-1}\overline{f}_1] \tag{9}$$

Since $\mathbf{M}_1$ and $\mathbf{M}_2$ are now mapped by $\mathbf{K}$,

$$\mathbf{M}_2 = \mathbf{K}\mathbf{M}_1 \tag{10}$$

The dynamic mode decomposition uses the singular value decomposition (SVD) to solve for $\mathbf{M}_1$. SVD factorizes the $\mathbf{M}$ matrix into a composition of three geometrical transformations, viz., $\mathbf{U}$ - the unitary matrix, $\mathbf{V}^*$ - the complex unitary matrix, and $\mathbf{\Sigma}$ - the scaling matrix.

Substituting for $\mathbf{M_1}$ in (10),

$$\mathbf{M_2} = \mathbf{K}\mathbf{U}\mathbf{\Sigma}\mathbf{V}^* \tag{11}$$

3) Predicting Frequency evolution using DMD: Using the Arnoldi iteration as $\mathbf{K}$ form a Krylov span, the companion matrix $\mathbf{H}$ can be substituted to replace the higher dimensional $\mathbf{K}$.

$$\tilde{\mathbf{H}}\omega = \sigma\omega \tag{12}$$

$$\mathbf{K}\mathbf{U} \approx \mathbf{U}\tilde{\mathbf{H}} \tag{13}$$

$$\mathbf{K}\mathbf{U} \approx \mathbf{U}\omega\sigma\omega^{-1} \tag{14}$$

$$\mathbf{K}(\mathbf{U}\sigma) \approx (\mathbf{U}\sigma)\sigma \tag{15}$$

σ presents the growth and/or decay rates and frequencies for the DMD modes. Using the initial conditions, $\overline{f}_1$ can be used to determine the scaling factor $\mathbf{b}$ as

$$\overline{f}_1 = \Psi\mathbf{b} \tag{16}$$

and $\mathbf{b}$ can be solved for using the Moore-Penrose pseudo-inverse,

$$\mathbf{b} = (\Psi * \Psi)^{-1}\Psi * \overline{f}_1 \tag{17}$$

the predicted frequency can be reconstructed by multiplying $\mathbf{b}$,

$$\hat{\mathbb{F}} = \Psi(V \circ \mathbf{b}) \tag{18}$$

G. Degraded Operational Performance Detection using Data-Driven Model

The centralized controller maintains the system stability by offsetting PV variability by dispatch the BESS using (5). However, when the communication network is experiencing high latency, the dispatch signal is delayed in reaching the BESS, preventing the successful execution of the control action. The low active power in the system causes the frequency to drop, and by the frequency setpoints defined by IEEE 1547 [32]for DERs, the remaining PV and BESS inverters drop out, causing system instability. During dynamic events, like the large change in PV output, the primary operational challenge is to maintain frequency stability [33], [34].

To compensate for the maloperation due to delay, we use the data-driven model from the DMD to predict frequency evolution using the terminal frequency measured as the initial conditions. The previous successful operation of the centralized control is fed as training data to the DMD module, and the $\mathbf{K}$ Koopman operator is obtained. Subsequently, the frequency predictions $\hat{\mathbb{F}}$ are compared with the measured frequency at the terminal controller. Norm-1 and Norm-2 errors are calculated between the measured and predicted frequency for each time step of the operation. Norm-1 error is the error between the sum of the absolute values of the measured and predicted frequency and Norm-2 is the error between the mean-square of

the measured and predicted frequency. The deviation from the measured and predicted frequency indicates the unsuccessful operation of the control, prompting the local controller to dispatch the setpoint provided via (6). When the deviations return to the acceptable range, the centralized MGC resumes being the primary controller in the scheme, ensuring that new setpoints based on the optimization are issued without stressing any particular resource.

IV. Results and Discussion

This section presents the test system and the operation of the delay-tolerant controller for the different modes of operation under two use cases.

A. Simulation Setup

The IEEE 123-node test system [35] is modified to represent three networked microgrids. Microgrids 1 and 2 have a combination of DG, PV, and BESS resources. The grid-following PV inverters were sized to pick up a significant amount of load during normal operating conditions. This ensures that the control algorithm can stress the generation dispatch of the BESS resources and make it more sensitive to delays in the battery actuation. If the loss of PV causes the frequency to drop below 56.5Hz, the IEEE 1547-2018 Standard specifies a clearing time of 160ms at which all DERs are required to trip.

The GridLAB-D simulation is set up such that at the simulation start, the test system is grid-connected and is allowed to operate at the rated frequency. At t = 500ms, an event generation trigger disconnects the utility bus at 150 by opening switch 13-152, initiating the islanding.

Switches 18-135, and 97-197 to form the networked microgrid MG-1 and MG-2, and the operation of switches 60-160 and 54-94 to form an individual island MG-3. Simultaneously, the microgrids are disconnected from being networked via the opening of switch 151-300, and since MG-3 does not have any dispatchable resource, it is entirely disconnected from the system. Subsequently, the system is now allowed to brought up to steady-state by the dispatch of the BESS and DGs to supply loads and maintain system frequency. The simulations run for 8000ms, with the loss of PV occurring at t = 4000ms. Three use cases evaluate the effect of system delays on the microgrid operation. The co-simulation was set up with GridLAB-D v4.3, NS-3 v3.3, Python 3.8, and Helics v2.7 on a violet Hat Linux server with 32 GB RAM, and 32 Core processor.

B. Case 1: System operation in Ideal Communication Network

In Case 1, the centralized controller successfully operates when an idealized communication network can operate with a fixed delay attribute typical to a point-to-point communication link. The fixed delay is due to the communication link delay plus the process delays due to the simulation of the NS-3 model and python optimization controller codes. The delay is low enough for the controller to receive the real power measurements from the GridLAB-D measurement endpoints, run the optimization and send the new setpoints to the GridLAB-D BESS endpoints within time such that the system was able to ride through the frequency drop contingency and maintain system stability as seen in Fig. 7.

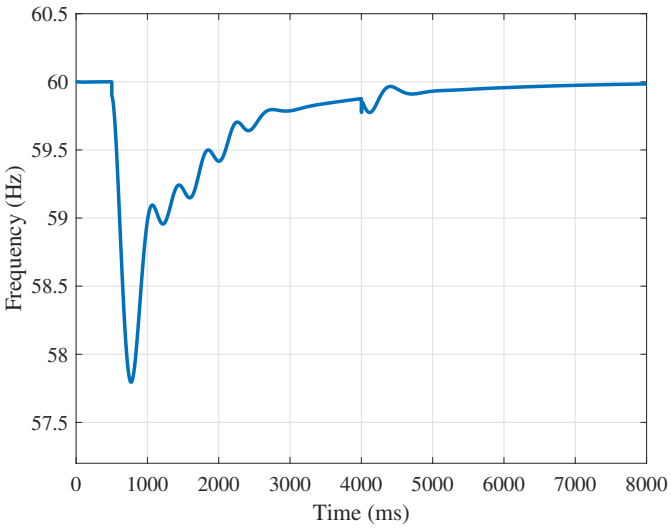

Fig. 7. Frequency of the system during ideal communications and successful operation of BESS

C. Training of the DMD model

Once the co-simulation of the power system model, communication system model and the centralized controller is performed for the system operation in an ideal communication network, data points of the terminal measurements of the inverter device are collected. As explained in section III-F, the time-series frequency measured at the inverter is used to train the DMD model. The trained model can now be used to predict the evolution of frequency in the absence of a control signal from the centralized control which is assumed to be due to latency in the communication network. The DMD model for each inverter resides in the terminal controller block that continuously tracks the difference between the measured and predicted frequency for each time step of the co-simulation. The terminal controller block is set up in the co-simulation as python federate that has end-points set up to read the measured terminal frequency of the controller for each time-step of the co-simulation.

D. Case 2: System operation in High Latency Communication Network with GFA operation

For Case 2, the same simulation setup is run in a non-ideal communication network where increased network traffic causes high delay. In addition to identical propagation and process delays seen in the ideal network, the network congestion introduces a high delay of around 200ms. The delay causes the frequency to drop below 57.2 Hz before the BESS could respond to the new setpoint signal. As mentioned earlier, the GFA loads capable of UFLS trip in response to the under-frequency contingency of 57.5Hz and 300 kW of GFA loads are lost as shown in Fig. 8. The action prevents the loss of system stability, but results in the loss of loads.

This article has been accepted for publication in a future issue of this journal, but has not been fully edited. Content may change prior to final publication. Citation information: DOI 10.1109/TSG.2022.3167436, IEEE Transactions on Smart Grid

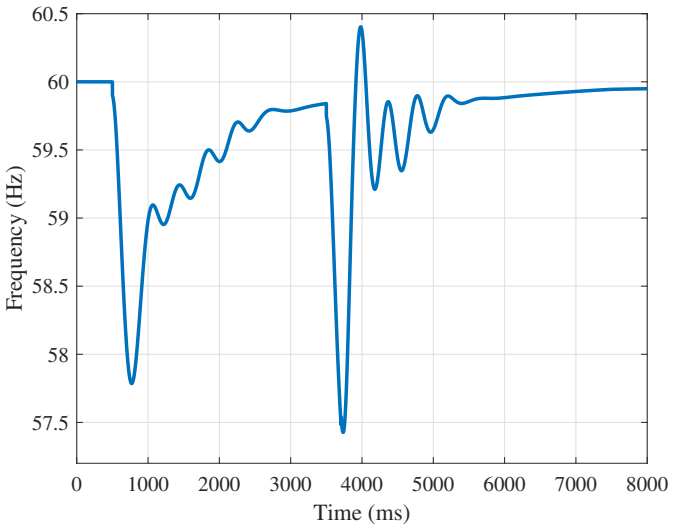

Fig. 8. Frequency of the system during non-ideal communications with GFA operation

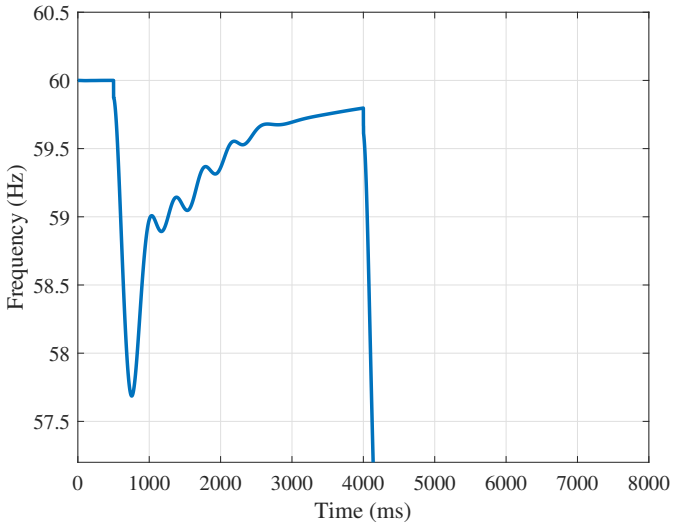

Fig. 9. Frequency of the system during ideal communications and successful operation of BESS

E. Case 3: System operation in High Latency Communication Network without GFA operation

In Case 3, the communication network delay causes the frequency to drop below the threshold of 56.5 Hz for 160s, causing the IEEE 1547 compliant inverters to trip in response to the under-frequency event as shown in Fig. 9. This is the worst-case scenario where the system stability is lost, and the entire microgrid experiences a blackout. The frequency trace in Fig. 9 stops around 4200ms due to the tripping of the inverters in GridLAB-D, causing the co-simulation to fail.

F. Operation of the Delay Tolerant Controller

The previous co-simulation results showed demonstrably that delays in the communication network cause the system to lose stability. The local controller at the BESS uses the time series frequency measurements obtained through the successful operation of the controller and builds the DMD-based linear operator for the prediction of frequency. A software trigger starts the prediction of frequency based on the previous successful operation. The result of the prediction block is shown in Fig. 10. The results indicate that the actuation of the BESS in regulating frequency is demonstrably reflected in the DMD-based frequency prediction. The local controller also concurrently calculates the new setpoint for the BESS based on the terminal frequency measurement per (6).

The observer block continuously monitors the two frequency data points: one measured at the terminal of the BESS and the other predicted via the DMD algorithm. These two data sets are analyzed for deviation, and the magnitude deviation allows the controller to identify the maloperation of the system due to communication system delay. Once the trajectory of the prediction shifts considerably from that of the measured frequency, the local controller accepts the internally calculated new dispatch setpoint for the BESS and discards the setpoint issued by the MGC. This causes the frequency to return to the nominal value, and the observer block returns control to the MGC. The delay-tolerant control operation prevents loss of loads, as seen in both Case 2 and Case 3. The loss of GFA loads is averted if a ULFS scheme exists, and a total microgrid outage is avoided if a UFLS scheme does not exist.

Two cases were studied with the delay-tolerant controls enabled. In Case A, the GFA loads are turned off, and the system behaves similar to Case 3. The DMD-based frequency prediction is compared with the terminal frequency at the BESS, and at times of high deviation, the operating mode of the system goes from 0 to 1, indicating a change from the centralized MGC to the local controller. Therefore, the local controller issues a more conservative battery dispatch value based on the droop and the BESS reserve capacity in the same time periods. The results of the Case A simulations are consolidated in Fig. 11.

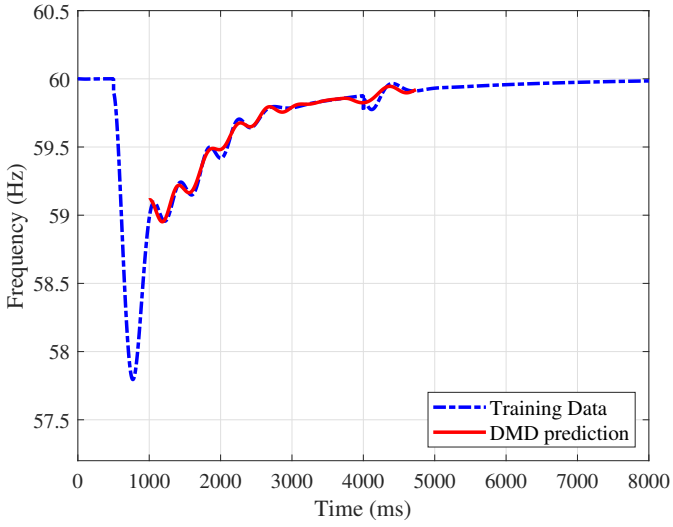

Fig. 10. DMD prediction of Frequency Evolution of Successful operation of BESS during Ideal Communications

This article has been accepted for publication in a future issue of this journal, but has not been fully edited. Content may change prior to final publication. Citation information: DOI 10.1109/TSG.2022.3167436, IEEE Transactions on Smart Grid

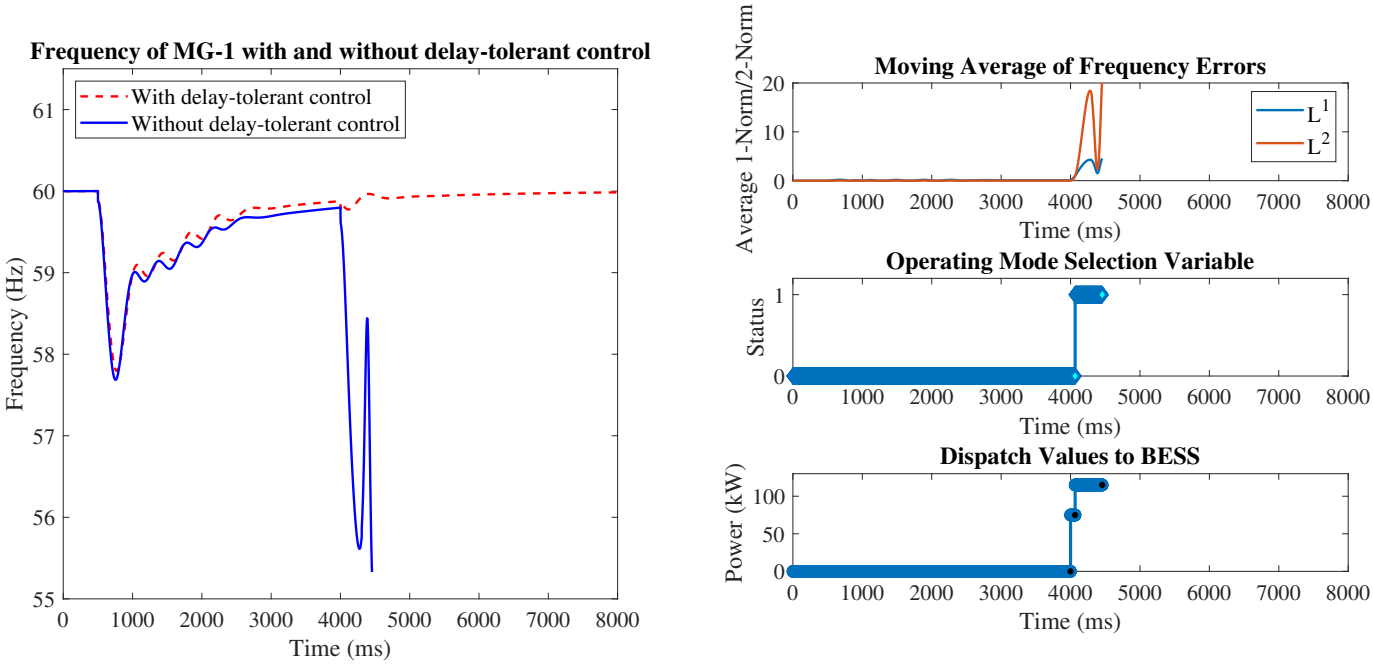

Fig. 11. Use case A: System operation is maintained with delay tolerant controller in high latency communication network. Dotted violet line in frequency plot is the predicted frequency to which the delay tolerant controller issues new set-points. Without delay tolerant control, the simulation fails around 4300 ms.

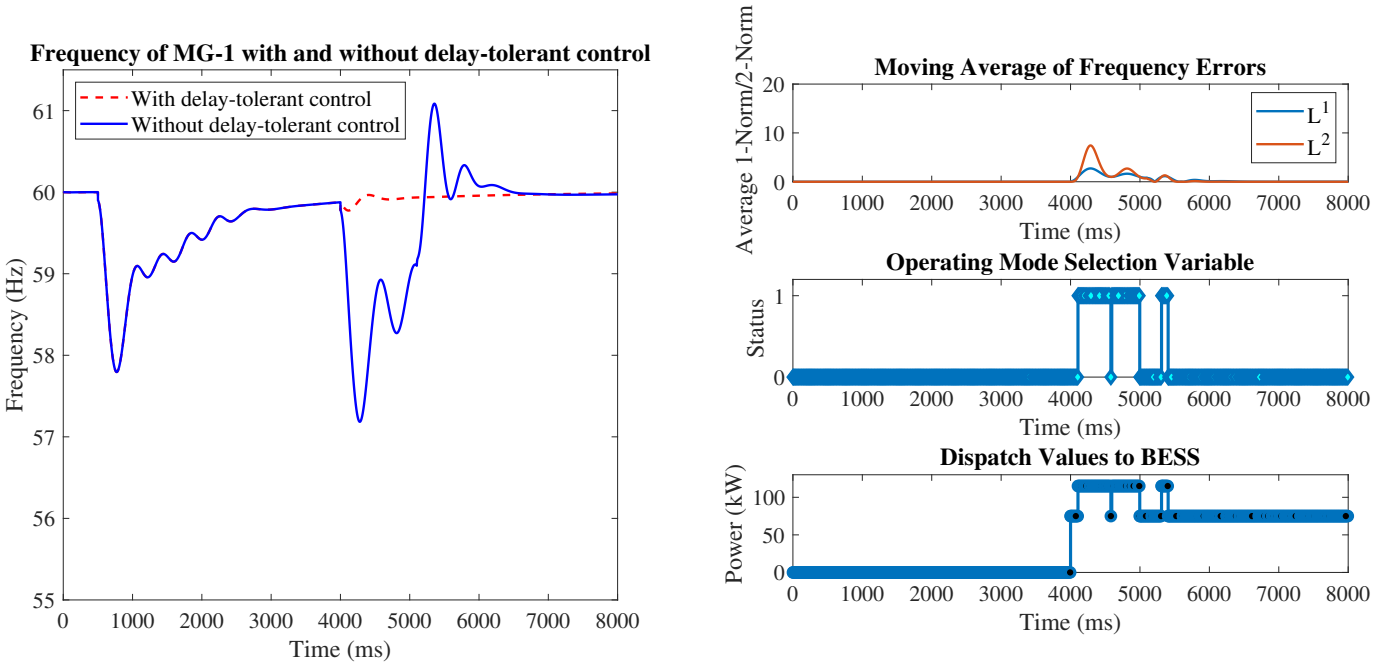

Fig. 12. Use Case B: Delay tolerant controller tracks predicted frequency and issues new setpoints to BESS. Though there is no loss of system stability in this use case, loss of GFA loads is prevented through the action of the delay tolerant controller.

For Case B, shown in Fig. 12, the communication network is congested to present a large latency value ($\approx$ 1000ms). The GFA loads are also enabled. As a result, without delay-tolerant controls, the BESS will have failed to respond to the MGC dispatch value, prompting the GFA loads to trip. At around 1s after the PV drops off, the BESS receives the MGC dispatch value, and the real power support provided by the BESS up-regulates the frequency to the nominal value. However, this would have caused the GFA loads to have tripped at 57.5 Hz, causing 300kW of load loss. With the delay-tolerant operation, the observer block can identify deviation in the frequency trajectory and dispatches the droop-based real power setpoint to the BESS when the deviation threshold is met. This instantly brings the system back to nominal frequency, and the load loss

due to GFA operation is avoided.

For both cases, the DMD algorithm is computationally fast and was able to predict the evolution of the inverter frequency for 200 time-steps in 4.19 milliseconds.

The resiliency scenario based on loss of load is shown in Fig. 13. The results indicate the preservation of resilient operation under communication network degradation with the use of the proposed delay-tolerant control algorithm. While the same microgrid operation lost 580kW without GFA enabled and 300kW with GFA enabled loads, the scenario did not see any loss of loads, in comparison, maintaining stability throughout the simulation time.

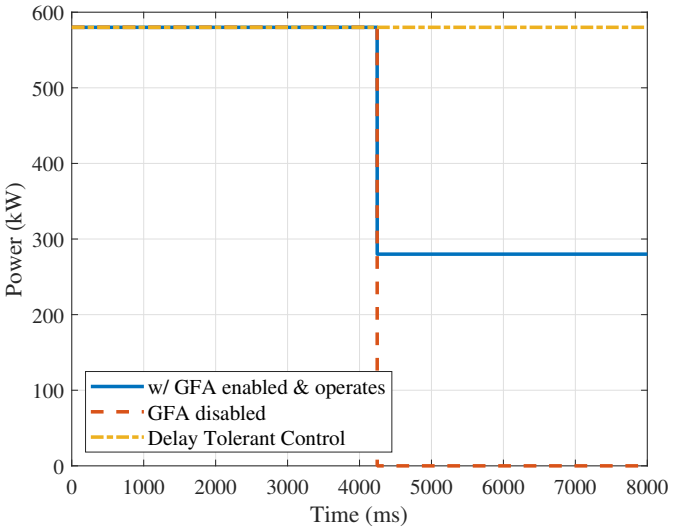

Fig. 13. Loads lost under different scenarios. No loss of load experienced when delay tolerant controller is implemented.

V. Conclusions

Microgrid resiliency increasingly relies on advanced controls executed over communication networks. However, latency in these communication networks can cause such controls to fail or work with reduced performance, thereby decreasing microgrid resiliency significantly. This paper proposes a data-driven algorithm to ensure the successful operation of controls to address this limitation. A HELICS co-simulation framework models and simulation is used for a specific use-case that demonstrably fails due to increased communication delays. A dynamic mode decomposition-based algorithm for predicting the evolution of frequency during a high impact, dynamic event (loss of PV resource), based on the successful historical operation, tracks the communication-assisted control's performance. The algorithm compares the predicted and measured frequency and selects between the BESS setpoint relayed via a communication system and a setpoint calculated locally at the inverter level based on terminal frequency measurement. With simulated delays in the communication system model, the algorithm prevents the loss of system stability by providing backup control of the BESS inverter resource. The proposed framework can assist system planners to economically under-design specific resources that can be supplemented by the resiliency-driven advanced controls capabilities. Delay tolerance can be utilized effectively when communication-assisted controls are layered onto existing legacy communication systems where utilities can face budgetary constraints in commissioning dedicated, high-reliability communication networks. The DMD algorithm provides improved insights into the non-successful control behavior of the system by accommodating the learned actuation of the central controller in a delayed communication system. In the future, other prediction algorithms for non-linear system evolution would be studied. Other use-cases that are sensitive to delays would also be explored and impact on BESS degradation will be analyzed with the proposed algorithm.

Acknowledgements

The authors would like to acknowledge the partial support from the WSU-PNNL Distinguished Graduate Research Fellowship (DGRP), WSU-PNNL Advanced Grid Institute (AGI), the National Science Foundation award 1932574, and the U.S. Department of Energy UI-ASSIST DE-IA0000025 project.

References

[1] *Accelerating Decarbonization of the US Energy System*. The National Academies Press: Washington, DC, USA, 2021.

[2] S. Liu, X. Wang, and P. X. Liu, "Impact of communication delays on secondary frequency control in an islanded microgrid," *IEEE Transactions on Industrial Electronics*, vol. 62, no. 4, pp. 2021–2031, 2014.

[3] Q. Shafiee, J. M. Guerrero, and J. C. Vasquez, "Distributed secondary control for islanded microgrids—a novel approach," *IEEE Transactions on power electronics*, vol. 29, no. 2, pp. 1018–1031, 2013.

[4] V. Nasirian, S. Moayedi, A. Davoudi, and F. L. Lewis, "Distributed cooperative control of dc microgrids," *IEEE Transactions on Power Electronics*, vol. 30, no. 4, pp. 2288–2303, 2014.

[5] J. W. Simpson-Porco, Q. Shafiee, F. Dörfler, J. C. Vasquez, J. M. Guerrero, and F. Bullo, "Secondary frequency and voltage control of islanded microgrids via distributed averaging," *IEEE Transactions on Industrial Electronics*, vol. 62, no. 11, pp. 7025–7038, 2015.

[6] M. Hosseinzadeh, L. Schenato, and E. Garone, "A distributed optimal power management system for microgrids with plug&play capabilities," *Advanced Control for Applications: Engineering and Industrial Systems*, vol. 3, no. 1, p. e65, 2021.

[7] A. Khorsandi, M. Ashourloo, and H. Mokhtari, "A decentralized control method for a low-voltage dc microgrid," *IEEE Transactions on Energy Conversion*, vol. 29, no. 4, pp. 793–801, 2014.

[8] E. Sortomme, S. Venkata, and J. Mitra, "Microgrid protection using communication-assisted digital relays," *IEEE Transactions on Power Delivery*, vol. 25, no. 4, pp. 2789–2796, 2009.

[9] V. Borozan, M. E. Baran, and D. Novosel, "Integrated volt/var control in distribution systems," in *2001 IEEE Power Engineering Society Winter Meeting. Conference Proceedings (Cat. No. 01CH37194)*, vol. 3. IEEE, 2001, pp. 1485–1490.

[10] J. Wu, T. Yang, D. Wu, K. Kalsi, and K. H. Johansson, "Distributed optimal dispatch of distributed energy resources over lossy communication networks," *IEEE Transactions on Smart Grid*, vol. 8, no. 6, pp. 3125–3137, 2017.

[11] B. Huang, L. Liu, H. Zhang, Y. Li, and Q. Sun, "Distributed optimal economic dispatch for microgrids considering communication delays," *IEEE Transactions on Systems, Man, and Cybernetics: Systems*, vol. 49, no. 8, pp. 1634–1642, 2019.

[12] J. Qi, Y. Kim, C. Chen, X. Lu, and J. Wang, "Demand response and smart buildings: A survey of control, communication, and cyber-physical security," *ACM Transactions on Cyber-Physical Systems*, vol. 1, no. 4, Oct. 2017. [Online]. Available: https://doi.org/10.1145/3009972

[13] M. Pau, E. Patti, L. Barbierato, A. Estebsari, E. Pons, F. Ponci, and A. Monti, "A cloud-based smart metering infrastructure for distribution grid services and automation," *Sustainable Energy, Grids and Networks*, vol. 15, pp. 14–25, 2018.

[14] K. De Craemer and G. Deconinck, "Analysis of state-of-the-art smart metering communication standards," in *Proceedings of the 5th young researchers symposium*, 2010.
[15] Y. Xu, C.-C. Liu, K. P. Schneider, F. K. Tuffner, and D. T. Ton, "Microgrids for service restoration to critical load in a resilient distribution system," *IEEE Transactions on Smart Grid*, vol. 9, no. 1, pp. 426–437, 2016.
[16] Federal Communications Commission, "FCC Report: Communications status report for areas impacted by hurricane maria," Sep 2017. [Online]. Available: https://docs.fcc.gov/public/attachments/DOC-346860A1.pdf
[17] P. Kansal and A. Bose, "Bandwidth and latency requirements for smart transmission grid applications," *IEEE Transactions on Smart Grid*, vol. 3, no. 3, pp. 1344–1352, 2012.
[18] F. Zhang, Y. Sun, L. Cheng, X. Li, J. H. Chow, and W. Zhao, "Measurement and modeling of delays in wide-area closed-loop control systems," *IEEE Transactions on Power Systems*, vol. 30, no. 5, pp. 2426–2433, 2015.
[19] P. T. Mana, K. P. Schneider, W. Du, M. Mukherjee, T. Hardy, and F. K. Tuffner, "Study of microgrid resilience through co-simulation of power system dynamics and communication systems," *IEEE Transactions on Industrial Informatics*, vol. 17, no. 3, pp. 1905–1915, 2021.
[20] Y.-K. Wu and K.-T. Tang, "Frequency support by bess–review and analysis," *Energy Procedia*, vol. 156, pp. 187–191, 2019.
[21] X. Wu, J. Zhao, and A. J. Conejo, "Optimal battery sizing for frequency regulation and energy arbitrage," *IEEE Transactions on Power Delivery*, 2021.
[22] D. Gräf, J. Marschewski, L. Ibing, D. Huckebrink, M. Fiebrandt, G. Hanau, and V. Bertsch, "What drives capacity degradation in utility-scale battery energy storage systems? the impact of operating strategy and temperature in different grid applications," *Journal of Energy Storage*, p. 103533, 2021.
[23] F. Conte, S. Massucco, G.-P. Schiapparelli, and F. Silvestro, "Day-ahead and intra-day planning of integrated bess-pv systems providing frequency regulation," *IEEE Transactions on Sustainable Energy*, vol. 11, no. 3, pp. 1797–1806, 2019.
[24] B. Bhattarai, L. Marinovici, M. Touhiduzzaman, F. K. Tuffner, K. P. Schneider, J. Xie, P. T. Mana, W. Du, and A. Fisher, "Studying impacts of communication system performance on dynamic stability of networked microgrid," *IET Smart Grid*, vol. 3, no. 5, pp. 667–676, 2020.
[25] B. Palmintier, D. Krishnamurthy, P. Top, S. Smith, J. Daily, and J. Fuller, "Design of the helics high-performance transmission-distribution-communication-market co-simulation framework," in *2017 Workshop on Modeling and Simulation of Cyber-Physical Energy Systems (MSCPES)*, 2017, pp. 1–6.
[26] Y. Li, Y. Qin, P. Zhang, and A. Herzberg, "Sdn-enabled cyber-physical security in networked microgrids," *IEEE Transactions on Sustainable Energy*, vol. 10, no. 3, pp. 1613–1622, 2018.
[27] P. A. Garcia, J. L. R. Pereira, S. Carneiro, V. M. Da Costa, and N. Martins, "Three-phase power flow calculations using the current injection method," *IEEE Transactions on power systems*, vol. 15, no. 2, pp. 508–514, 2000.
[28] K. P. Schneider, F. K. Tuffner, M. A. Elizondo, C.-C. Liu, Y. Xu, S. Backhaus, and D. Ton, "Enabling resiliency operations across multiple microgrids with grid friendly appliance controllers," *IEEE Transactions on Smart Grid*, vol. 9, no. 5, pp. 4755–4764, 2017.
[29] S. Tirunagari, S. Kouchaki, N. Poh, M. Bober, and D. Windridge, "Dynamic mode decomposition for univariate time series: analysing trends and forecasting," 2017.
[30] A. R. Teixeira, A. M. Tomé, M. Bohm, C. G. Puntonet, and E. W. Lang, "How to apply nonlinear subspace techniques to univariate biomedical time series," *IEEE Transactions on Instrumentation and Measurement*, vol. 58, no. 8, pp. 2433–2443, 2009.
[31] P. J. Schmid, L. Li, M. P. Juniper, and O. Pust, "Applications of the dynamic mode decomposition," *Theoretical and Computational Fluid Dynamics*, vol. 25, no. 1, pp. 249–259, 2011.
[32] "IEEE standard for interconnection and interoperability of distributed energy resources with associated electric power systems interfaces," *IEEE Std 1547-2018 (Revision of IEEE Std 1547-2003)*, pp. 1–138, 2018.
[33] P. Kundur, J. Paserba, V. Ajjarapu, G. Andersson, A. Bose, C. Canizares, N. Hatziargyriou, D. Hill, A. Stankovic, C. Taylor, T. Van Cutsem, and V. Vittal, "Definition and classification of power system stability ieee/cigre joint task force on stability terms and definitions," *IEEE Transactions on Power Systems*, vol. 19, no. 3, pp. 1387–1401, 2004.
[34] M. Farrokhabadi, C. A. Cañizares, J. W. Simpson-Porco, E. Nasr, L. Fan, P. A. Mendoza-Araya, R. Tonkoski, U. Tamrakar, N. Hatziargyriou, D. Lagos, R. W. Wies, M. Paolone, M. Liserre, L. Meegahapola, M. Kabalan, A. H. Hajimiragha, D. Peralta, M. A. Elizondo, K. P. Schneider, F. K. Tuffner, and J. Reilly, "Microgrid stability definitions, analysis, and examples," *IEEE Transactions on Power Systems*, vol. 35, no. 1, pp. 13–29, 2020.
[35] K. P. Schneider, B. Mather, B. Pal, C.-W. Ten, G. J. Shirek, H. Zhu, J. C. Fuller, J. L. R. Pereira, L. F. Ochoa, L. R. de Araujo *et al.*, "Analytic considerations and design basis for the ieee distribution test feeders," *IEEE Transactions on power systems*, vol. 33, no. 3, pp. 3181–3188, 2017.

Gowtham Kandaperumal is a Senior Engineer with Commonwealth Edison (ComEd), Il working in the Reliability group. He received his PhD in Electrical Engineering and Computer Science from Washington State University in 2021 and his Masters degree in Electrical Engineering from Arizona State University in 2014. Prior to ComEd, he was a Distinguished Graduate Research Fellow at Pacific Northwest National Laboratory (2019-2021) and an Electrical Engineer at Affiliated Engineers Inc. (2014-2017).

Kevin P. Schneider (Fellow, IEEE) received the B.S. degree in physics and the M.S. and Ph.D. degrees in electrical engineering from the University of Washington. He is currently a Laboratory Fellow at the Pacific Northwest National Laboratory, the Manager of the Distribution and Demand Response Sub-Sector, and a Research Professor at Washington State University as part of the PNNL/WSU Advanced Grid Institute (AGI). He is an Affiliate Associate Professor at the University of Washington and a licensed Professional Engineer in WA, USA. His main research interests include distribution system analysis and power system operations. He is the past Chair of the Power & Energy Society (PES) Distribution System Analysis (DSA) Sub-Committee and the Analytic Methods for Power Systems (AMPS) Committee.

Anurag K. Srivastava (S'99, M'05, SM'09, F'22) is a Raymond J. Lane Professor and Chairperson of the Computer Science and Electrical Engineering Department at the West Virginia University. He is also an adjunct professor at the Washington State University and senior scientist at the Pacific Northwest National Lab. He received his Ph.D. degree in power engineering from the Illinois Institute of Technology in 2005. His research interest includes data-driven algorithms for power system operation and control including resiliency analysis. He is serving as vice-chair of IEEE PES power system operation SC, and vice-chair of tools for power grid resilience TF. He is an IEEE Fellow, PES Distinguished Lecturer and the author of more than 300 technical publications including a book on power system security and 4 patents.